



Cite this: DOI: 10.1039/d1cy00366f

Efficient acceptorless dehydrogenation of hydrogen-rich N-heterocycles photocatalyzed by Ni(OH)₂@CdSe/CdS quantum dots†

Yanpeng Liu,^{ab} Tianjun Yu,^{id}*^a Yi Zeng,^{id}^{ab} Jinping Chen,^{id}^a
Guoqiang Yang^{id}^{bc} and Yi Li^{id}*^{ab}

Hydrogen storage using liquid organic hydrogen carriers (LOHCs) is a promising hydrogen storage technology; however, the hydrogen release process typically requires a high temperature. Developing dehydrogenation technology under mild conditions is highly desirable. Herein, a new approach for photocatalytic acceptorless dehydrogenation of hydrogen-rich LOHCs using Ni(OH)₂@CdSe/CdS QDs as the photocatalyst was demonstrated. 1,2,3,4-Tetrahydroquinoline (THQ), iso-THQ, indoline, and their derivatives were selected as hydrogen-rich substrates, which exhibit excellent dehydrogenation efficiency with the release of hydrogen photocatalyzed by Ni(OH)₂@CdSe/CdS QDs. Up to 100% yields of hydrogen and over 90% yields of complete dehydrogenation products were obtained at ambient temperature. Isotope tracer studies indicate a stepwise pathway, beginning with the photocatalytic oxidation of the substrate to release a proton and followed by proton exchange with heavy water. This work provides a promising alternative strategy to develop highly efficient, low cost and earth-abundant photocatalysts for acceptorless dehydrogenation of hydrogen-rich LOHCs.

Received 1st March 2021,
Accepted 15th April 2021

DOI: 10.1039/d1cy00366f

rsc.li/catalysis

Introduction

As an environmentally friendly, abundant and high energy density gas fuel, hydrogen is an ideal candidate energy carrier to address environmental pollution and energy shortage in the world.^{1–5} Although the concept of “hydrogen economy” has been put forward by many governments as a strategy to complete the nation's transformation toward the hydrogen energy society, a great challenge facing the implementation is how to store and transport hydrogen safely and efficiently.⁶ Liquid hydrogen storage and high-pressure hydrogen storage are the most common methods in use at present, but both methods run the risk of hydrogen leaks and explosions.⁷ Recent developments in hydrogen storage have provided

evidence that the liquid organic hydrogen carrier (LOHC) technology is a very attractive alternative, because it makes high density hydrogen storage possible at ambient temperature and pressure.^{8–12} The LOHC technology involves reversible hydrogenation and acceptorless dehydrogenation between hydrogen-poor and hydrogen-rich organic liquids, achieving storage and release of hydrogen. Most studies on LOHC systems focused on the hydrogen capacity and the efficiency of acceptorless dehydrogenation reactions between hydrogen-poor and hydrogen-rich pairs. Benzene/*cyclo*-hexane, toluene/methylcyclohexane and naphthalene/decalin are the most studied hydrogen-poor/hydrogen-rich pairs because of their high theoretical hydrogen capacity, but high reaction temperatures are required for high conversion efficiency.^{13–19} Several groups have made efforts to decrease the reaction enthalpy by introducing nitrogen atoms,^{20–24} but the temperature of thermocatalytic dehydrogenation reactions is still higher than 110 °C. In order to avoid the inconvenience caused by the temperature of thermally promoted reactions, light-induced acceptorless dehydrogenation reaction may become an alternative way.

Tanaka, Crabtree, Field, and Saito are the pioneers in the field of photocatalytic acceptorless dehydrogenation from alkanes using noble metals iridium and rhodium or cheap metal iron and cobalt complexes.^{25–28} Because of the great energy barrier for the C(sp³)-H band activation of alkanes, reactions previously reported in the literature are inefficient and

^a Key Laboratory of Photochemical Conversion and Optoelectronic Materials, Technical Institute of Physics and Chemistry, Chinese Academy of Sciences, Beijing, 100190, China. E-mail: tianjun_yu@mail.ipc.ac.cn, yili@mail.ipc.ac.cn

^b University of Chinese Academy of Sciences, Beijing, 100049, P. R. China

^c Key Laboratory of Photochemistry, Institute of Chemistry, Chinese Academy of Sciences, Beijing, 100190, P. R. China

† Electronic supplementary information (ESI) available: GC-FID analyses of THQ and QL, GC-TCD analyses of H₂ and D₂, XPS survey and high-resolution XPS spectra of CdSe/CdS QDs and Ni(OH)₂@CdSe/CdS QDs, control experiments of the photocatalytic hydrogen release over Ni(OH)₂@CdSe/CdS QDs, time dependent photocatalytic H₂ and D₂ release over Ni(OH)₂@CdSe/CdS QDs, and ESI-MS spectra of dehydrogenation products. See DOI: 10.1039/d1cy00366f

require ultraviolet light to initiate.^{29–31} Recently, several examples of photocatalytic dehydrogenation of hydrogen-rich organic liquids have demonstrated that the reaction efficiency has increased dramatically by replacing alkanes with N-heterocycles.^{32–35} However, noble metals are often indispensable in these systems, such as ruthenium, platinum, palladium, and so on. Further, a homogenous system is greatly limited in application by the tedious synthesis and recyclability process of these costly noble metal complexes. To date, h-BCN, MoS₂/ZnIn₂S₄, and Pd/TiO₂ have been reported as heterogeneous catalysts for the photocatalytic acceptorless dehydrogenation of N-heterocycles.^{36–38} However, h-BCN and MoS₂/ZnIn₂S₄ are effective only for the dehydrogenation of tetrahydroquinolines and tetrahydroisoquinolines, and Pd/TiO₂ contains precious metals. Therefore, developing an economical, efficient heterogeneous photocatalytic acceptorless dehydrogenation system is still highly desirable.

CdSe/CdS core-shell quantum dots (QDs) have received significant attention in the past few decades because of their fascinating lower cost, earth-abundant optical and electronic properties.^{39–41} Herein, we for the first time report an efficient photocatalytic acceptorless dehydrogenation of hydrogen-rich N-heterocycles (tetrahydroquinolines, tetrahydroisoquinolines and indolines) catalyzed by surface Ni(OH)₂-loaded CdSe/CdS core-shell QDs (Ni(OH)₂@CdSe/CdS). Tetrahydroquinoline and indoline derivatives are dehydrogenated to their corresponding N-heteroaromatics with excellent yields, accompanied by the release of hydrogen upon blue light irradiation. This work provides a new strategy for photocatalytic acceptorless dehydrogenation of hydrogen-rich organic liquids, as well as clear experimental evidence on the dehydrogenation mechanism, demonstrating potential for application to LOHC technology.

Experimental

Materials

If not specially indicated, reagents and solvents were used as commercially available without further purification. Ultrapure water with an 18.2 MΩ cm resistivity (Millipore) was used for all experiments.

Synthesis of CdSe QDs

CdSe QDs stabilized by 3-mercaptopropionic acid were made according to the reported methods.⁴² Firstly, 40 mg Se powder (0.5 mmol) was transferred to a Na₂SO₃ (100 mL, 15 mM) aqueous solution. Then, the resulting mixture was degassed by evacuating and then refluxed until the Se powder was dissolved completely to obtain a transparent Na₂SeSO₃ solution. Colloidal MPA-CdSe QDs were prepared by introducing a freshly prepared Na₂SeSO₃ (10 mL, 5 mM) solution into a 190 mL N₂-saturated solution containing CdCl₂·2.5H₂O and MPA at pH 11.0. The concentration of Cd²⁺ was set to be 1 mM, and the feed ratios of Cd:MPA:Se were 1:1.5:0.25. The resulting reaction mixture was immediately

refluxed under N₂-saturated conditions to generate CdSe QDs of desired sizes controlled by the refluxing time of 3.0 h.

Synthesis of CdSe/CdS QDs

CdSe QDs are used as the core materials to prepare CdSe/CdS core-shell QDs *in situ*. Firstly, the pre-prepared MPA-CdSe QDs were purified to remove the extra ligands and impurities in water by precipitation method. A stock solution of 200 mL MPA-CdSe QDs was concentrated to 20 mL and then was precipitated by adding an excessive amount of isopropanol. The obtained precipitate was dispersed by using 200 mL redistilled water and then was heated to 50 °C under an N₂ atmosphere with vigorous stirring. Na₂S (60 mL, 5 mM) and CdCl₂·2.5H₂O (40 mL, 5 mM) aqueous solutions were in turn pumped into the CdSe QD solution with a speed of 20 mL min⁻¹ and 15 mL min⁻¹, respectively. After the addition of these precursors, the solution was reacted for another 2 h to ensure the growth of CdSe/CdS QDs.

Characterization and measurements

Absorption and photoluminescence spectra were measured with a Shimadzu UV-2550PC spectrometer and a Hitachi F-4600 spectrometer, respectively. X-ray diffraction patterns were obtained by using a Bruker D8 Focus under Cu-Kα radiation. High-resolution transmission electron microscopy (HRTEM) images were obtained by using a JEM-2100F microscope with an accelerating voltage of 200 kV. X-ray photoelectron spectroscopy (XPS) was carried out on a Thermo ESCALAB 250 XPS spectrophotometer with Al-Kα radiation. The binding energy scale was calibrated using the C 1s peak at 284.8 eV. Photoelectrochemical and cyclic voltammetry measurements were performed on a CHI 760E in a standard three electrode cell. Working electrodes were designed by adding ethanol and Nafion suspension containing CdSe/CdS QDs or Ni(OH)₂@CdSe/CdS QDs onto glassy carbon electrodes and 2 cm² area of clean FTO for electrochemical impedance spectroscopy (EIS) and transient photocurrent response measurements, respectively. ESI-MS results were obtained using a Waters Q-TOF Premier apparatus.

Photocatalytic dehydrogenation experiments

To a glass reactor containing a magnetic stirring bar was added CdSe/CdS QDs, NiCl₂·6H₂O, H₂O/CH₃CN (V/V = 2/3, 5 mL) and hydrogen-rich N-heterocycles. The solution was degassed *in vacuo* and refilled with N₂ 3 times in an ice-water bath, and then 2 mL ultrapure CH₄ was injected into the system to work as the internal standard for quantitative GC analysis. Then the reaction mixture was stirred for 24 h upon 420 nm LED irradiation (*I* = 50 mW cm⁻²) at ambient temperature. The gas phase was analysed for the H₂ yield by GC-TCD using a 5 Å molecular sieve column (2 m × 2 mm) and N₂ as the carrier gas. The gas phase was analysed for the D₂ yield by GC-TCD using a 15% MnCl₂@γ-Al₂O₃ column (2 m × 2 mm) and He as the carrier gas. Then the generated dehydrogenation products were analysed by GC-FID using an SH-Rtx-5 column (30 m × 0.25

mm) and N_2 as the carrier gas. Later on, $Ni(OH)_2@CdSe/CdS$ QDs were separated from the reaction mixture by centrifugation at 8000 r min^{-1} for 5 min, and the products were confirmed by ESI-MS.

Results and discussion

The formation of the CdSe/CdS core-shell structure was confirmed by a series of characterization techniques. Typical excitonic peaks of CdSe and CdSe/CdS QDs at 433 nm and 452 nm can be observed in their UV-vis absorption spectra (Fig. 1a), accompanied with a bathochromic shift of emission caused by the CdS shell formation (Fig. 1b).⁴³ The band-gap energies (E_g) are estimated to be 2.66 and 2.60 eV for CdSe and CdSe/CdS QDs from their Tauc plots, respectively (Fig. 1c), indicating that the CdS shell enhances the visible-light harvesting ability. The X-ray diffraction (XRD) patterns demonstrate that the characteristic peaks corresponding to the (111), (220) and (311) planes located at 25.4° , 42.0° , and 49.7° for CdSe shift to 26.0° , 43.3° , and 50.8° for CdSe/CdS, moving consistently toward the values of CdS QDs (Fig. 1d). The transmission electron microscopy (TEM) and high-resolution TEM (Fig. 1e and f) images show that the CdSe QDs are nearly spherical nanoparticles with an average diameter of 3.0 nm, while the obtained CdSe/CdS QDs have an ellipsoidal shape with an average width and length of 3.5 and 5.0 nm. The interplanar spacings of the (111) crystal plane are 0.353 nm and 0.338 nm for CdSe and CdSe/CdS QDs, respectively. Moreover, the (220) crystal plane of cubic CdS with a lattice spacing of 0.207 nm was also found in the CdSe/CdS QDs, giving another strong evidence of the formation of CdSe/CdS core/shell QDs.

In order to evaluate the performance of CdSe and CdSe/CdS QDs, photocatalytic acceptorless dehydrogenation of 1,2,3,4-tetrahydroquinoline (THQ) to quinoline (QL) was conducted. A reaction system consisting of the CdSe or CdSe/CdS core-shell QDs and the substrate THQ was dispersed in acetonitrile-water binary solvent *via* a 30 min ultrasound treatment before the photocatalytic reaction. The photocatalytic dehydrogenation reaction was started by injecting a certain amount of $NiCl_2$ into the reaction systems upon 420 nm light irradiation with a 50 mW cm^{-2} intensity. Both the CdSe and CdSe/CdS QDs catalytic systems show hydrogen release upon irradiation, and the amount of hydrogen released is closely related to the irradiation time, as shown in Fig. 2a. The control experiments indicated that no hydrogen release was observed in the absence of irradiation, or CdSe or CdSe/CdS QDs, indicating that they are essential, and $NiCl_2$ itself cannot act as a photocatalyst alone for the dehydrogenation reaction. The photocatalytic activity of the CdSe QD system can only last for 12 h, and that of the CdSe/CdS QD system remains almost unchanged for 24 h under the experimental conditions, demonstrating that the CdSe/CdS core-shell QDs are more stable during the photocatalytic dehydrogenation of THQ. The effects of CdSe/CdS QD and $NiCl_2$ concentrations on the yield of dehydrogenation were also investigated. The yields of 39% for the formation of QL and 44% for the hydrogen release were obtained by gas chromatography using 20 mM THQ, 0.6 mg mL^{-1} CdSe/CdS QDs and 0.4 mM $NiCl_2$ in H_2O/CH_3CN (V/V = 2/3) mixed solvent. Further optimization experiments for the amount of CdSe/CdS QDs and $NiCl_2$ were conducted to improve the yield of QL by varying one condition while keeping all the other conditions identical. The yield of QL increases with the

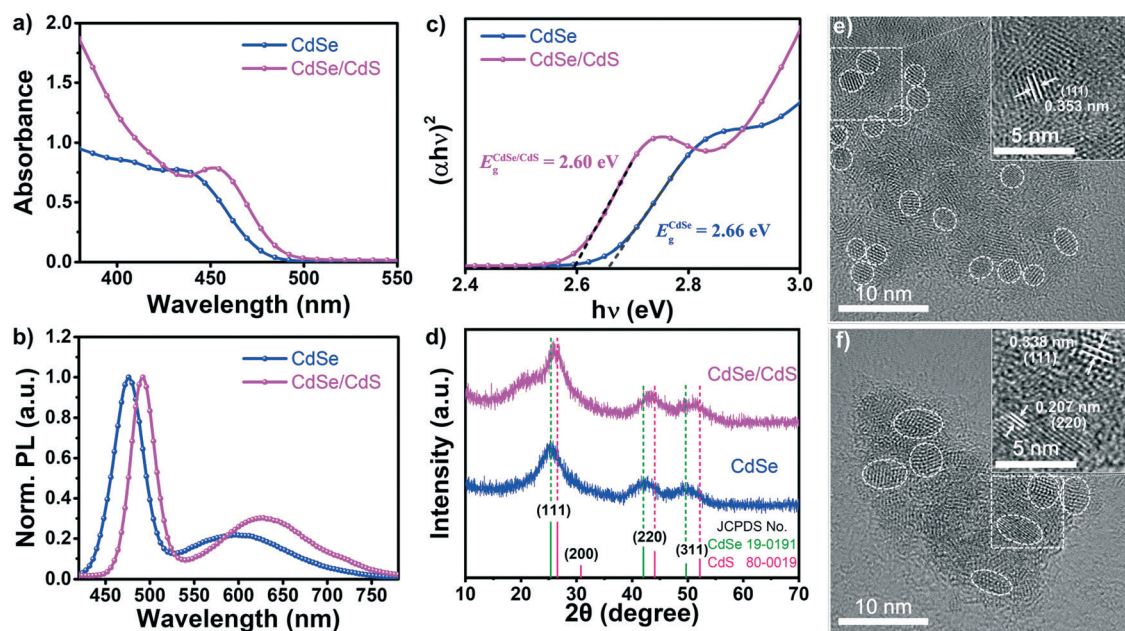


Fig. 1 (a and b) Absorption and normalized emission spectra of CdSe and CdSe/CdS QDs. The emission spectra were obtained under 400 nm excitation. (c) Tauc plots of CdSe and CdSe/CdS QDs. (d) XRD patterns of CdSe and CdSe/CdS QDs. (e and f) TEM and HRTEM (inset) images of CdSe and CdSe/CdS QDs.

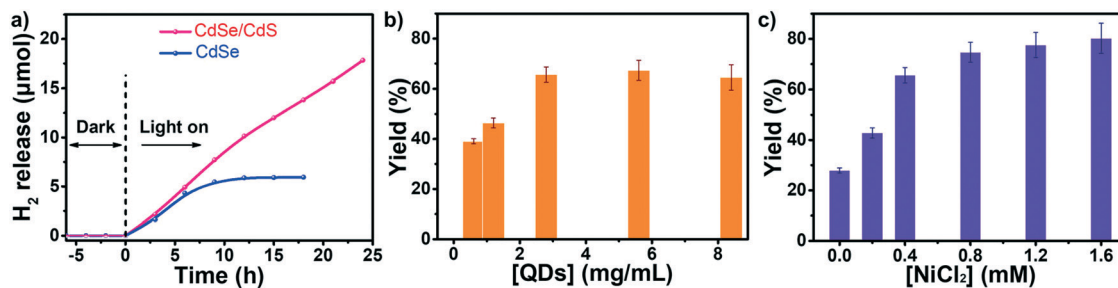


Fig. 2 (a) Time dependent photocatalytic hydrogen release over CdSe and CdSe/CdS QDs, respectively ($[\text{CdSe}] = [\text{CdSe/CdS}] = 0.5 \text{ mg mL}^{-1}$, $[\text{NiCl}_2] = 0.2 \text{ mM}$, $[\text{THQ}] = 20 \text{ mM}$). (b) Influence of the concentration of CdSe/CdS QDs on the photocatalytic dehydrogenation of THQ ($[\text{NiCl}_2] = 0.4 \text{ mM}$, $[\text{THQ}] = 20 \text{ mM}$). (c) Influence of the concentration of NiCl_2 on the photocatalytic dehydrogenation of THQ ($[\text{CdSe/CdS}] = 2.8 \text{ mg mL}^{-1}$, $[\text{THQ}] = 20 \text{ mM}$). The photocatalytic reactions were performed in $\text{H}_2\text{O}/\text{CH}_3\text{CN}$ ($V/V = 2/3$) for 24 h under blue LED irradiation ($\lambda = 420 \text{ nm}$, $I = 50 \text{ mW cm}^{-2}$).

concentration of CdSe/CdS QDs when the concentration is below 2.8 mg mL^{-1} (Fig. 2b), which can be ascribed to more photons absorbed by the reaction system. Further increasing the concentration of CdSe/CdS QDs results in no improvement of the QL yield, which may be caused by two possible reasons: 1) the redundant increase of CdSe/CdS QDs for the limited incident photons and 2) the self-quenching caused by high concentration of CdSe/CdS QDs. Fig. 2c and S1 and S2[†] demonstrate that the presence of NiCl_2 can significantly increase the dehydrogenation efficiency. In the absence of NiCl_2 , the yield of QL is only 28% after 24 hours of irradiation. The yield of QL increases with the increase in the concentration of NiCl_2 , and reaches 80% at a NiCl_2 concentration of 1.6 mM,

indicating that the presence of NiCl_2 enhances the photocatalytic activity of dehydrogenation. The ESI-MS of the reaction mixture (Fig. S3[†]) after removing the photocatalyst by centrifugation further proved that THQ was completely dehydrogenated to QL instead of partially dehydrogenating to 1,2-dihydroquinoline or 3,4-dihydroquinoline.

The high photocatalytic activity of acceptorless dehydrogenation of THQ encouraged us to explore the application of this photocatalytic system to other substrates. THQ derivatives and several other N-heterocycles were examined under the optimal conditions ($[\text{CdSe/CdS}] = 2.8 \text{ mg mL}^{-1}$, $[\text{NiCl}_2] = 1.6 \text{ mM}$, $\text{H}_2\text{O}/\text{CH}_3\text{CN}$ ($V/V = 2/3$), and the results are summarized in Table 1. 2-MeTHQ and 4-MeTHQ (THQ bearing

Table 1 Acceptorless dehydrogenation of hydrogen-rich N-heterocycles

Entry ^a	Substrate	Product	Time (h)	Conversion ^b (%)	GC yield ^b (%)	H ₂ yield ^c (%)
1			24	95	80	95
2			24	97	82	94
3			24	100	88	100
4			24	71	47	61
5			24	64	38	59
6			24	85	78	72
7			24	100	86	100
8			12	100	93	100
9			12	98	92	98

^a Reaction conditions: hydrogen-rich N-heterocycles (20 mM), CdSe/CdS QDs (2.8 mg mL^{-1}), NiCl_2 (1.6 mM), and $\text{H}_2\text{O}/\text{CH}_3\text{CN}$ ($V/V = 2/3$, 5 mL), under irradiation with 420 nm LEDs at room temperature ($I = 50 \text{ mW cm}^{-2}$). ^b Conversions and yields were determined by GC-FID analysis using a peak area normalization method. ^c Hydrogen yields were determined by GC-TCD analysis using CH_4 as the internal standard.

2-methyl and 4-methyl groups) were converted to their corresponding 2-MeQL and 4-MeQL in 82% and 88% yields, respectively (entries 2 and 3). Meanwhile, the hydrogen yields were up to 94% and 100%, which are very close to the conversions of the substrate. The adsorption of the dehydrogenation products on the surface of CdSe/CdS QDs may be responsible for their lower yields than conversion. The higher conversions of 2-MeTHQ and 4-MeTHQ than that of THQ are attributed to stabilization by the methyl group, which is similar to previous results in the literature.⁴⁴ When the aromatic ring was substituted with a methoxyl group at the 7 position, 7-MeOQL was obtained only in 47% yield (entry 4). The substrates were also extended to tetrahydroisoquinoline (iso-THQ) and its derivatives. The photocatalytic dehydrogenation of iso-THQ produces isoquinoline (iso-QL) in only 38% yield (entry 5). The low yield of iso-QL can be ascribed to the difficult oxidation process of iso-THQ caused by nonconjugation of the secondary amine with the phenyl group.⁴⁵ When the electron donating substituents methyl and phenyl were attached to the 1 position, 1-methyl and 1-phenylisoquinolines were obtained in 78 and 86% yields, respectively (entries 6 and 7), which also benefits from the stabilization by the substituents. Notably, the dehydrogenation reactions of tetrahydroisoquinolines are complete rather than partial, which is concluded from the ESI-MS analysis of the reaction mixture (Fig. S4–S9[†]). More exciting results were obtained by using indoline and 2-methyl indoline substrates. The GC yields of indole and 2-methylindole were as high as 93% and 92%, accompanied with the generation of hydrogen in 100% and 98% yield, respectively (entries 8 and 9), which can be ascribed to their single hydrogen removal process.

The optimization experiments demonstrate that NiCl₂ plays a crucial role in the improvement of the photocatalytic activity. To investigate the behavior of NiCl₂ during the photocatalytic reaction, we have analyzed the catalyst composition after photocatalytic dehydrogenation reaction by means of scanning TEM (STEM) and elemental mapping analysis (Fig. 3a–f). The elemental mapping images show that the photocatalyst is composed of Cd, Se, S and Ni elements. The high consistency of Ni distribution with other elements indicates that Ni is deposited on the surface of the CdSe/CdS QDs in the photocatalytic reaction system, which is further validated by X-ray photoelectron spectroscopy (XPS) measurements. The specific bonding and chemical states of Ni were also analyzed by XPS (Fig. 3g and S10 and S11[†]). As shown in Fig. 3g, the high-resolution XPS spectrum of Ni 2p reveals two typical peaks located at 856.7 and 874.2 eV, which are consistent with the Ni 2p_{3/2} and Ni 2p_{1/2} spin-orbit peaks of Ni(OH)₂, respectively.^{46,47} Two peaks located at 862.1 and 880.3 eV are assigned to the corresponding satellite peaks of Ni(OH)₂. These indicate that NiCl₂ converts to Ni(OH)₂ on the surface of the CdSe/CdS QDs, forming Ni(OH)₂@CdSe/CdS QDs. The *in situ* formed Ni(OH)₂ captures electrons from the CdSe/CdS QDs and becomes a new active site for proton reduction because of the less negative potential of Ni²⁺/Ni than that of CdS,⁴⁸ thus greatly improving the catalytic activity of the photocatalyst.

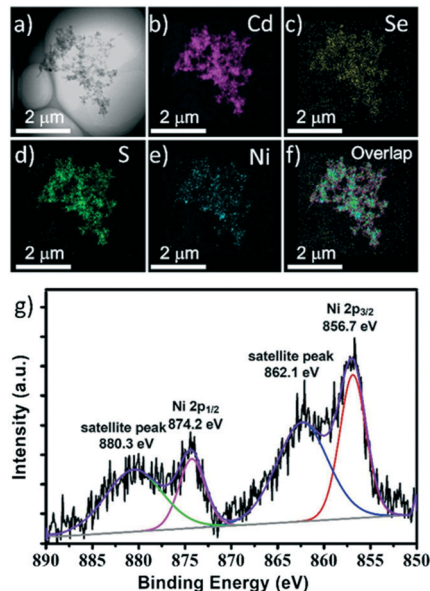


Fig. 3 (a–f) STEM image and the corresponding elemental mapping images of the Ni(OH)₂@CdSe/CdS QDs obtained from the photocatalytic system after 24 hours of irradiation. (g) High-resolution XPS spectrum of Ni 2p distributed on the surface of Ni(OH)₂@CdSe/CdS QDs.

To gain an insight into the electronic level structure, we carried out cyclic voltammetry (CV) measurements to analyse the valence band (E_{VB}) of CdSe and CdSe/CdS QDs, which is approximately equal to that of the oxidation potential (E_{pa}).⁴⁹ Both of them exhibit an E_{pa} approximate to 1.10 V (vs. NHE), corresponding to the E_{VB} of the CdSe QDs (Fig. S12[†]). Additionally, the CdSe/CdS QDs present another E_{pa} of approximately 1.49 V, corresponding to the E_{VB} of the CdS shell. Considering that the conduction band (E_{CB}) is equal to the difference between E_{VB} and E_g , the E_{CB} of the CdSe QDs is calculated to be -1.56 V. The E_{CB} of the CdS shell is estimated to be -1.50 V by the difference between the E_{VB} of the CdSe core and the E_g of the CdSe/CdS QDs, which is attributed to the spatially indirect transition from the valence band of the CdSe core to the lowest conduction band of the CdS shell.^{43,50} Obviously, the CdSe/CdS QDs formed a quasi-type II carrier distribution (Fig. 4), which is beneficial for

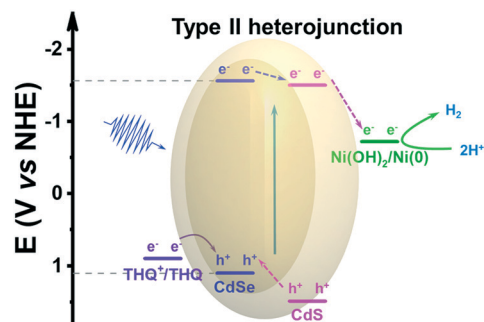


Fig. 4 Energy level diagram of the proposed mechanism for the photocatalytic acceptorless dehydrogenation of THQ by Ni(OH)₂@CdSe/CdS QDs.

improving the charge separation efficiency.^{43,51,52} After absorbing photons, electrons and holes are generated and transferred to the conduction band of the CdS shell and the valence band of CdSe, respectively. Since the reduction potential (E_{RE}) of Ni(OH)₂ (-0.72 V)⁵³ is more positive than the E_{CB} of the CdS shell, the electron transfer from the CdS shell to the catalyst Ni(OH)₂ is thermodynamically feasible. The emission of CdSe/CdS QDs is dramatically quenched by Ni(OH)₂ (Fig. S13[†]), indicating that the electron transfer occurs.^{54,55} THQ is directly oxidized by the holes randomly distributed on the surface of the CdSe/CdS QDs, because the E_{VB} of the CdSe/CdS QDs is more positive than the E_{pa} of THQ (Fig. S14[†]). Transient photocurrent response and electrochemical impedance spectroscopy (EIS) measurements of the CdSe/CdS QDs and Ni(OH)₂@CdSe/CdS QDs were performed to investigate the interfacial charge transport behavior. As shown in Fig. 5a, the transient photocurrent response of the Ni(OH)₂@CdSe/CdS QDs are remarkably higher than that of the CdSe/CdS QDs, indicating the more effective separation and transition of the photoinduced electron/hole pairs. The Nyquist plot of the Ni(OH)₂@CdSe/CdS QDs in the dark exhibits a smaller semicircular arc diameter compared to that of the CdSe/CdS QDs (Fig. 5b), suggesting a lower charge-transfer resistance.

Understanding the mechanism of the hydrogen release process will lead to designing active photocatalysts for the acceptorless dehydrogenation of hydrogen-rich LOHCs. Hence, an isotope tracer experiment was conducted by replacing H₂O-CH₃CN with a D₂O-CH₃CN mixed solvent to identify the elementary steps in the acceptorless

dehydrogenation of THQ over Ni(OH)₂@CdSe/CdS QDs. After 24 hours of irradiation, only deuterium gas (D₂) was detected in the gas phase of the reaction system, accompanied with the production of QL and the consumption of THQ in the liquid phase (Fig. S15 and S16[†]). The reaction carried out in pure acetonitrile solvent hardly detected the formation of H₂ and QL. Obviously, the removal of hydrogen from THQ is not in the form of H₂. A reasonable inference is that THQ is firstly oxidized and then releases a proton. The released protons exchange rapidly with D₂O, and the produced deuterons are reduced to D₂. No H₂ product detected in the gas phase can be ascribed to the large amount of D₂O in the system and the quick exchange reaction, indicating that almost all released protons are converted to deuterons. Even though a trace amount of protons exists in the system, the generated H₂ is lower than the detection limit of gas chromatography. On the basis of the isotope tracer studies, the photocatalytic dehydrogenation and the control experiments, a possible mechanism for the photocatalytic acceptorless dehydrogenation of THQ is proposed and illustrated in Scheme 1. Upon photoexcitation of Ni(OH)₂@CdSe/CdS QDs, a valence band hole and a conduction band electron are produced. The substrate is then oxidized by the hole to generate the corresponding cation radical, which was indirectly proved through the formation of an adduct with 5,5-dimethyl-1-pyrroline N-oxide (DMPO) by ESI-MS (Fig. S17[†]). Following the deprotonation of the cation radical, another electroneutral intermediate is formed. The electroneutral intermediate undergoes the second photosensitized oxidation and deprotonation process in turn to form a double bond in a nitrogenous six-membered ring, which was confirmed by the partial dehydrogenation product signal in the ESI-MS spectrum (Fig. S8[†]). Subsequent isomerization allows the partially dehydrogenated intermediate to be continually oxidized by the valence band holes and to remove protons. After four oxidation and deprotonation processes, the initial hydrogen-rich substrate eventually becomes an unsaturated organic hydrogen carrier. The protons detached from the substrate

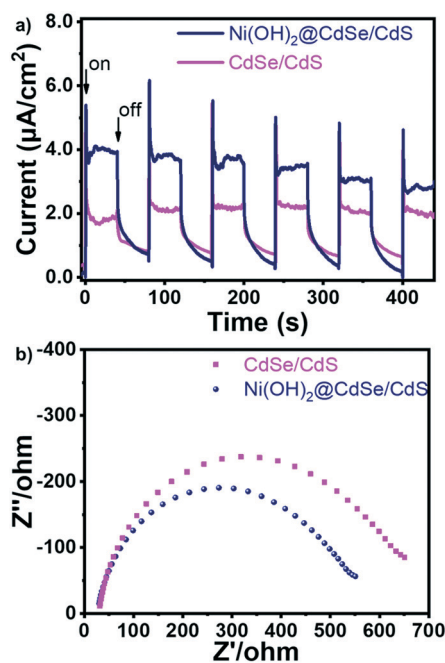
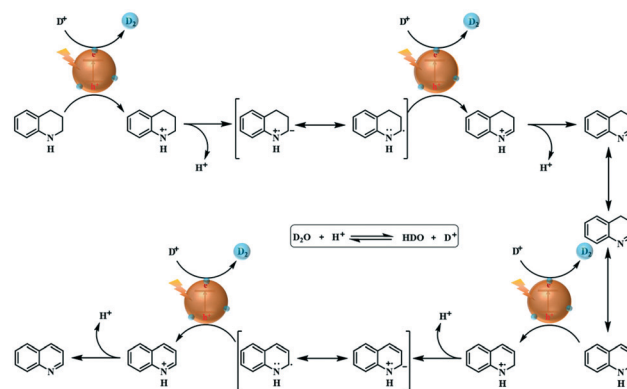


Fig. 5 (a) The transient photocurrent response of CdSe/CdS QDs and Ni(OH)₂@CdSe/CdS QDs upon visible-light illumination ($\lambda \geq 420$ nm). (b) Nyquist plot of CdSe/CdS QDs and Ni(OH)₂@CdSe/CdS QDs.



Scheme 1 Proposed mechanism for the photocatalytic acceptorless dehydrogenation of THQ catalyzed by Ni(OH)₂@CdSe/CdS QDs.

exchange with heavy water, and then, with the help of the cocatalyst Ni(OH)₂ deposited on the surface of the CdSe/CdS QDs, D⁺ is reduced to form D₂.

Conclusion

In summary, an efficient photocatalyst based on Ni(OH)₂@CdSe/CdS QDs has been reported for its activity toward acceptorless dehydrogenation of hydrogen-rich N-heterocycles. Ni(OH)₂@CdSe/CdS QDs are proved to be highly active for the photocatalytic dehydrogenation of THQ, iso-THQ, indoline, and their derivatives, with as high as 93% yield of dehydrogenation products and 100% yield of released hydrogen. The admirable activity of the photocatalytic system can be attributed to the heterojunction structure of the CdSe/CdS QDs and the suitable redox potential of the Ni(OH)₂ co-catalysts. As a consequence, the combination of these photocatalysts raises the possibility that this system might be applied to hydrogen release at ambient temperature. The present research provides a powerful complement or potential competitor to the thermally promoted dehydrogenation systems, especially suitable for the application in a sunny environment.

Author contributions

Yanpeng Liu: investigation, formal analysis, writing – original draft. Tianjun Yu: conceptualization, supervision, writing – review & editing, funding acquisition. Yi Zeng: supervision, funding acquisition. Jinping Chen: supervision. Guoqiang Yang: supervision. Yi Li: conceptualization, writing – review & editing, supervision, funding acquisition.

Conflicts of interest

There are no conflicts to declare.

Acknowledgements

This work is supported by the National Natural Science Foundation of China (No. 21672226, 21673264, 21573266, 22090012, and U20A20144), and the Strategic Priority Research Program of Chinese Academy of Sciences (No. XDB17000000).

Notes and references

- S. S. Chen, T. Takata and K. Domen, *Nat. Rev. Mater.*, 2017, **2**, 17050.
- J. Li, H. Li, G. M. Zhan and L. Z. Zhang, *Acc. Chem. Res.*, 2017, **50**, 112–121.
- Y. M. Shi and B. Zhang, *Chem. Soc. Rev.*, 2016, **45**, 1529–1541.
- X. X. Zou and Y. Zhang, *Chem. Soc. Rev.*, 2015, **44**, 5148–5180.
- T. J. Yu, Y. Zeng, J. P. Chen, Y. Y. Li, G. Q. Yang and Y. Li, *Angew. Chem., Int. Ed.*, 2013, **52**, 5631–5635.
- P. Makowski, A. Thomas, P. Kuhn and F. Goettmann, *Energy Environ. Sci.*, 2009, **2**, 480–490.
- D. J. Durbin and C. Malardier-Jugroot, *Int. J. Hydrogen Energy*, 2013, **38**, 14595–14617.
- E. M. Lane, N. Hazari and W. H. Bernskoetter, *Chem. Sci.*, 2018, **9**, 4003–4008.
- E. Gianotti, M. Taillades-Jacquín, J. Roziere and D. J. Jones, *ACS Catal.*, 2018, **8**, 4660–4680.
- P. T. Aaldto-Saksa, C. Cook, J. Kiviaho and T. Repo, *J. Power Sources*, 2018, **396**, 803–823.
- P. Preuster, C. Papp and P. Wasserscheid, *Acc. Chem. Res.*, 2017, **50**, 74–85.
- Q. L. Zhu and Q. Xu, *Energy Environ. Sci.*, 2015, **8**, 478–512.
- S. Hodoshima, H. Nagata and Y. Saito, *Appl. Catal., A*, 2005, **292**, 90–96.
- A. S. Fung, M. J. Kelley, D. C. Koningsberger and B. C. Gates, *J. Am. Chem. Soc.*, 1997, **119**, 5877–5887.
- J. V. Pande, A. Shukla and R. B. Biniwale, *Int. J. Hydrogen Energy*, 2012, **37**, 6756–6763.
- Z. J. Xia, H. F. Lu, H. Y. Liu, Z. k. Zhang and Y. F. Chen, *Catal. Commun.*, 2017, **90**, 39–42.
- F. Alhumaidan, D. Cresswell and A. Garforth, *Energy Fuels*, 2011, **25**, 4217–4234.
- A. Shukla, J. V. Pande and R. B. Biniwale, *Int. J. Hydrogen Energy*, 2012, **37**, 3350–3357.
- G. Lee, Y. Jeong, B.-G. Kim, J. S. Han, H. Jeong, H. B. Na and J. C. Jung, *Catal. Commun.*, 2015, **67**, 40–44.
- R. Yamaguchi, C. Ikeda, Y. Takahashi and K.-i. Fujita, *J. Am. Chem. Soc.*, 2009, **131**, 8410–8412.
- D. Forberg, T. Schwob, M. Zaheer, M. Friedrich, N. Miyajima and R. Kempe, *Nat. Commun.*, 2016, **7**, 13201.
- S. Chakraborty, W. W. Brennessel and W. D. Jones, *J. Am. Chem. Soc.*, 2014, **136**, 8564–8567.
- G. Jaiswal, V. G. Landge, D. Jagadeesan and E. Balaraman, *Nat. Commun.*, 2017, **8**, 2147.
- Y. H. Han, Z. Y. Wang, R. R. Xu, W. Zhang, W. X. Chen, L. R. Zheng, J. Zhang, J. Luo, K. L. Wu, Y. Q. Zhu, C. Chen, Q. Peng, Q. Liu, P. Hu, D. S. Wang and Y. D. Li, *Angew. Chem., Int. Ed.*, 2018, **57**, 11262–11266.
- M. J. Burk, R. H. Crabtree and D. V. McGrath, *J. Chem. Soc., Chem. Commun.*, 1985, 1829–1830.
- M. V. Baker and L. D. Field, *J. Am. Chem. Soc.*, 1987, **109**, 2825–2826.
- K. Nomura and Y. Saito, *J. Chem. Soc., Chem. Commun.*, 1988, 161–162.
- T. Sakakura, T. Sodeyama, Y. Tokunaga and M. Tanaka, *Chem. Lett.*, 1988, 263–264.
- J. A. Maguire, W. T. Boese and A. S. Goldman, *J. Am. Chem. Soc.*, 1989, **111**, 7088–7093.
- A. D. Chowdhury, N. Weding, J. Julis, R. Franke, R. Jackstell and M. Beller, *Angew. Chem., Int. Ed.*, 2014, **53**, 6477–6481.
- J. G. West, D. Huang and E. J. Sorensen, *Nat. Commun.*, 2015, **6**, 10093.
- K. H. He, F. F. Tan, C. Z. Zhou, G. J. Zhou, X. L. Yang and Y. Li, *Angew. Chem., Int. Ed.*, 2017, **56**, 3080–3084.
- S. Kato, Y. Saga, M. Kojima, H. Fuse, S. Matsunaga, A. Fukatsu, M. Kondo, S. Masaoka and M. Kanai, *J. Am. Chem. Soc.*, 2017, **139**, 2204–2207.

- 34 Z. B. Jia, Q. Yang, L. Zhang and S. Z. Luo, *ACS Catal.*, 2019, **9**, 3589–3594.
- 35 M. K. Sahoo and E. Balaraman, *Green Chem.*, 2019, **21**, 2119–2128.
- 36 M. F. Zheng, J. L. Shi, T. Yuan and X. C. Wang, *Angew. Chem., Int. Ed.*, 2018, **57**, 5487–5491.
- 37 M. M. Hao, X. Y. Deng, L. Z. Xu and Z. H. Li, *Appl. Catal., B*, 2019, **252**, 18–23.
- 38 N. O. Balayeva, Z. Mamiyev, R. Dillert, N. Zheng and D. W. Bahnemann, *ACS Catal.*, 2020, **10**, 5542–5553.
- 39 O. Chen, J. Zhao, V. P. Chauhan, J. Cui, C. Wong, D. K. Harris, H. Wei, H.-S. Han, D. Fukumura, R. K. Jain and M. G. Bawendi, *Nat. Mater.*, 2013, **12**, 445–451.
- 40 X. L. Dai, Y. Z. Deng, X. G. Peng and Y. Z. Jin, *Adv. Mater.*, 2017, **29**, 1607022.
- 41 A. P. Alivisatos, *Science*, 1996, **271**, 933–937.
- 42 X. B. Li, Y. J. Gao, Y. Wang, F. Zhan, X. Y. Zhang, Q. Y. Kong, N. J. Zhao, Q. Guo, H. L. Wu, Z. J. Li, Y. Tao, J. P. Zhang, B. Chen, C. H. Tung and L. Z. Wu, *J. Am. Chem. Soc.*, 2017, **139**, 4789–4796.
- 43 Z. J. Li, X. B. Fan, X. B. Li, J. X. Li, F. Zhan, Y. Tao, X. Y. Zhang, Q. Y. Kong, N. J. Zhao, J. P. Zhang, C. Ye, Y. J. Gao, X. Z. Wang, Q. Y. Meng, K. Feng, B. Chen, C. H. Tung and L. Z. Wu, *J. Mater. Chem. A*, 2017, **5**, 10365–10373.
- 44 X. T. Sun, J. Zhu, Y. T. Xia and L. Wu, *ChemCatChem*, 2017, **9**, 2463–2466.
- 45 N. Zumbraegel, M. Sako, S. Takizawa, H. Sasai and H. Groeger, *Org. Lett.*, 2018, **20**, 4723–4727.
- 46 J. G. Yu, S. H. Wang, B. Cheng, Z. Lin and F. Huang, *Catal. Sci. Technol.*, 2013, **3**, 1782–1789.
- 47 Y. P. Zhang, Z. L. Jin, X. Yan, H. Y. Wang and G. R. Wang, *Catal. Lett.*, 2019, **149**, 1174–1185.
- 48 X. P. Chen, S. Chen, C. F. Lin, Z. Jiang and W. F. Shangguan, *Int. J. Hydrogen Energy*, 2015, **40**, 998–1004.
- 49 S. K. Haram, A. Kshirsagar, Y. D. Gujarathi, P. P. Ingole, O. A. Nene, G. B. Markad and S. P. Nanavati, *J. Phys. Chem. C*, 2011, **115**, 6243–6249.
- 50 S. Y. Jin, J. Zhang, R. D. Schaller, T. Rajh and G. P. Wiederrecht, *J. Phys. Chem. Lett.*, 2012, **3**, 2052–2058.
- 51 J. A. Nasir, Z. u. Rehman, S. N. A. Shah, A. Khan, I. S. Butler and C. R. A. Catlow, *J. Mater. Chem. A*, 2020, **8**, 20752–20780.
- 52 W. N. Nan, Y. Niu, H. Y. Qin, F. Cui, Y. Yang, R. C. Lai, W. Z. Lin and X. G. Peng, *J. Am. Chem. Soc.*, 2012, **134**, 19685–19693.
- 53 C. G. Zoski, *Handbook of Electrochemistry*, Elsevier, Amsterdam, the Netherlands, 2006.
- 54 J. A. Nasir, M. Hafeez, M. Arshad, N. Z. Ali, I. F. Teixeira, I. McPherson, R. Zia Ur and M. A. Khan, *ChemSusChem*, 2018, **11**, 2587–2592.
- 55 J. A. Nasir, N. Islam, Z. u. Rehman, I. S. Butler, A. Munir and Y. Nishina, *Mater. Chem. Phys.*, 2021, **259**, 124140.